Wasit Journal of Engineering Sciences

Journal homepage: https://ejuow.uowasit.edu.iq

Performance Evaluation of Bidirectional SEPIC-ZETA DC-DC Converter with Different Ambient Temperature

Nuha A. AL-Obaidi[1], Hasan Fahad Khazaal[1], Riyadh A. Abbas[1]

Affiliations
1Department of Electrical Engineering, Wasit University, Wasit, Iraq

Correspondence
Nuha A. AL-Obaidi,
Department of Electrical Engineering, Wasit University, Wasit, Iraq
Email: nuhaa302@uowasit.edu.iq

Received
06-June-2022
Revised
4-September-2022
Accepted
06-September-2022

Doi: 10.31185/ejuow.Vol10.Iss3.340

Abstract
Bidirectional DC-DC converters allow power to be transferred in any direction between two electrical sources. These converters are increasingly employed in a variety of applications, including battery chargers and dischargers, energy storage devices, electrical vehicle motor drives, aircraft power systems, telecom power supplies, and others, due to their ability to reverse the direction of power flow. One of these basic types of bidirectional DC-DC converters is the SEPIC-ZETA converter. In this paper, the structure of this converter has been studied when MOSFET power switches are employed. Also, an electrical thermal analysis, which is based on the ambient temperature (between 25 °C and 40 °C), has been employed by using two MOSFET models (UJ3C065080K3S and SCT50N120). The study shows the effects of utilizing different MOSFET models on power losses and thermal analysis. According to the simulation results, the junction temperature of the MOSFET was 151.38 °C in the forwarding mode and for the first model (UJ3C065080K3S) at T = 40 °C, while the MOSFET junction temperature was 158.5 °C in the backward mode. In the second model (SCT50N120) and at the same T = 40°C, the MOSFET junction temperature exceeds 130.6°C in the forwarding mode. When the converter was operating in backward mode, its junction temperature was 128.7 °C. The bidirectional SEPIC-ZETA converter performs better in the second model of the MOSFET (SCT50N120).

Keywords: Bidirectional DC-DC, thermal, DC-DC converter, SEPIC-ZETA converter, PLECS.

الخلاصة: تسمح محولات DC-DC ثنائية الاتجاه بنقل الطاقة في أي اتجاه بين مصدرين كهربائيين. تم استخدام هذا النوع من المحولات في الاونة الاخيرة بشكل متزايد في كثير من التطبيقات ، بما في ذلك شواحن البطاريات وأجهزة التفريغ ، وأجهزة تخزين الطاقة ، و محركات السيارات الكهربائية ، وأنظمة طاقة الطائرات ، وإمدادات الطاقة للاتصالات ، وغيرها ، نظرًا لقدرة هذه المحولات على عكس اتجاه سريان الطاقة. الدائرة الخاصة بالمحول SEPIC-ZETA ثنائي الاتجاه تم توضيحها في هذا البحث ، بما في ذلك التحليل الحراري و الكهربائي الخاص بها. يعتمد التحليل الحراري على درجة الحرارة البيئة المحيطة (25°C و 40°C). تم استخدام الMOSFET في هذه الدائرة. في هذا البحث تم استخدام نموذجين مختلفين لل MOSFET هي (UJ3C065080K3S) و (SCT50N120) وذلك لدراسة تاثير هذين النموذجين على الخسائر في القدرة الكهربائية وكذلك تحليل حراري ومعرفة تاثير حرارة الجو على درجة حرارة الMOSFET. اظهرت نتائج المحاكاة ، ان درجة حرارة الوصلة لل MOSFET هي 151.38 درجة مئوية عند العمل بالاتجاه الامامي وللنموذج الأول (UJ3C065080K3S) عند درجة حرارة البيئة المحيطة (40) درجة مئوية ، بينما كانت درجة حرارة الوصلة لل MOSFET هي 158.5 درجة مئوية عند العمل بالاتجاه العكسي. اما في النموذج الثاني (SCT50N120)ونفس درجة الحرارة للبيئة المحيطة T = 40 درجة مئوية ، تجاوزت درجة حرارة الوصلة لل MOSFE 130.6 درجة مئوية بالاتجاه الامامي. كانت درجة حرارة الوصلة المحول 128.7 درجة مئوية عندما يكون العمل بالاتجاه المعاكس.

1. INTRODUCTION

Bidirectional DC-DC Converters (BDCs) have gained researchers' interest recently, especially in microgrids. BDCs have emerged as a promising option for a variety of applications, including portable devices, spacecraft power systems, Uninterruptible Power Supplies (UPS), electric vehicles, fuel cells, and renewable energy systems, in addition to their traditional applications in energy storage and DC motor drives [1, 2]. BDCs are used in battery chargers and dischargers to regulate the discharger's output voltage to a specified value when using the battery's

stored energy. [3]. Non-isolated bidirectional DC-DC converters are less complex to use and more efficient than isolated converters, so they are preferable when galvanic isolation is not required [4]. Depending on the state of charge and current direction of the battery, the duty cycle of the converter manages charging and discharging. To store energy in a battery and link it to the DC microgrid, a non-isolated bidirectional DC-DC converter was designed and simulated. If Photovoltaic (PV) power is available throughout the day, the DC-DC converter charges the batteries in buck mode, and when PV power is not available, the battery discharges, allowing the converter to supply power to the DC load in boost mode [5]. One of the basic types of non-isolated BDCs discussed in this paper is a bidirectional SEPIC-ZETA DC-DC converter. It could be seen as just a hybrid of the basic SEPIC and ZETA converters. The suggested converter not only has the capability of bidirectional power flow but also has low switching and conduction losses. This converter is also suitable for application in distributed power. The SEPIC/ZETA converter is a low-cost, non-inverting DC-DC converter capable of buck or boost operation [6]. The remainder of the paper is presented as follows: the following part discusses related works. The bidirectional SEPIC-ZETA DC-DC converter architecture was discussed in the third part. The fourth section presents an evaluation of the work using PLECS, and the last section provides a conclusion to this paper.

2. RELATED WORK

A summary of recent developments in the bidirectional DC-DC converters thermal and electrical model is described as follows:

In [7] a SEPIC/ZETA converter was used to reduce output voltage ripple and eliminate voltage fluctuations during switching. The voltage control method is a fuzzy logic controller, which is supposed to give a steady output. The bidirectional SEPIC/ZETA converter has been shown to work well in both SEPIC and ZETA modes. The fuzzy logic controller operates well when energy is transferred to storage energy and when stored energy is supplied to the load.

In [8] the goal of this paper is building a 1.5kW buck converter with a switching frequency of 100kHz and a 350V DC input. The performance of commercially available GaN devices is compared in terms of packaging, conduction, and switching losses. At all current parameters, the module achieves above 97 % efficiency. The gate charge method and PSPICE simulation are used to calculate losses for the eGaN and cascade GaN switches. The performance of e-GaN is slightly better than that of cascade GaN. A unique heatsink assembly has been developed for thermal management that provides efficient heat extraction as well as cost savings.

In [9] the authors use newly created loss models to compare the efficiency of three-level, two-level, and interleaved bidirectional buck/boost converters in a drive cycle. The analysis indicated that a three-level converter has higher overall efficiency. As a proof of concept, a 1 kW prototype was constructed and produced. The results show that a three-level converter improves efficiency significantly, especially at switching frequencies higher than 100 kHz.

In [10] this research began by offering a model for calculating the converter's efficiency theoretically. After that, the impact of temperature, duty cycle, switching frequency, and switching device material on the converter's efficiency is examined. (1) the effectiveness of the switching frequency of 15 kHz is approximately 2% greater than that of 25 kHz, according to the analysis of the experimental data. (2) at 25 °C, the MOSFET SiC's efficiency is comparable to that of the IGBT Si in both buck and boost modes, whereas the efficiency of the IGBT Si is 2% greater at 25° C than at 85 °C. (3) in buck mode, peak efficiencies fall from 97.6 % to 90.3 % as duty cycles decrease from 66.7 % to 33.33 %. When the duty cycle is increased from 33.33 % to 75% in boost mode, peak efficiency falls from 96.9% to 96.5% and then to 92.41%. (4) the proposed model can accurately compute the converter's efficiency.

In [11] proposed to employ a model-based approach to create modern hybrid and fully powered automobiles with a bidirectional onboard charger (OBC) device. The research's major purpose and contribution is to incorporate both electrical and thermal modeling of switching devices in the same simulation environment. The created models are assessed under various operational settings for validation of practical significance and the reliability of the established control algorithms under varied operating conditions. A comprehensive robustness study of the parametric modifications of the model with regard to the nominal case also helps to validate the models and control loops. The operational limits of the specified devices and components are maintained in all simulations, in terms of electrical and thermal behavior, their features are listed on data sheets. Predictive health care

solutions based on recent machine learning and artificial intelligence concepts can be established due to the creation of a model that is both accurate and efficient in terms of computing.

However, since all of the previously presented designs have good characteristics, the main differences and contributions of this paper are listed as follows:

1. While the researchers improved power switch models and investigated thermal losses and efficiency at various ambient temperatures, no attempt has been made to investigate the impact of this temperature on the junction temperature of MOSFETs and diodes, as well as how these ambient temperatures could damage power switche (MOSFET). Therefore, the effect of the environmental temperature has been studied in detail.

2. Improving the basic bidirectional DC-DC converters (BDCs) by adding or removing components is employed to improve performance, efficiency, low output voltage or current ripples,etc.. However, the majority of researchers use Matlab software for implementation rather than other tools such as PLECS, which is used for implementation in this paper.

3. PRINCIPALS OPERATION OF BIDIRECTIONAL SEPIC-ZETA CONVERTOR

There are two modes of operation for the bidirectional SEPIC-ZETA DC-DC converter that is presented in Figure.1.

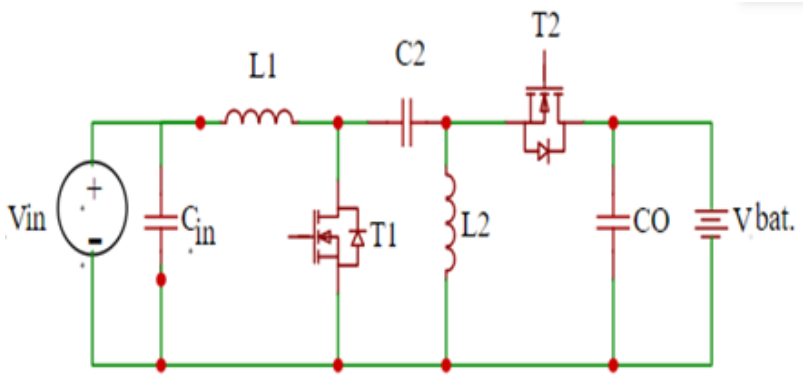

Figure 1 bidirectional SEPIC-ZETA DC-DC converter

In the first case, if the output of the renewable source is adequate to supply the load, the bidirectional converter is in charging mode (SEPIC mode), and power flows from the DC bus to the battery, as shown in Figure.2a. If the source's output voltage is outside the permissible range in the second case, the load is fed from the ESS. The bidirectional DC-DC converter is in discharging mode (Zeta mode), as shown in Figure. 2b, and power flows from the battery to the DC bus [12].

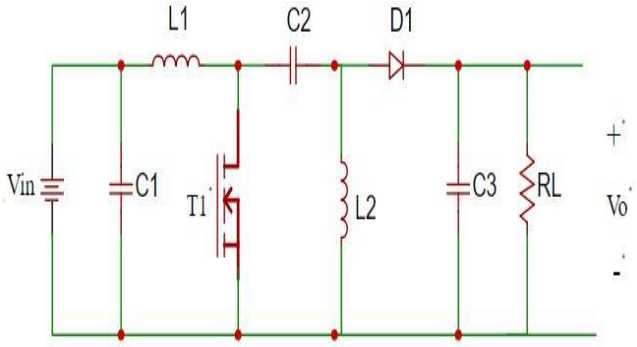

Figure 2a SEPIC mode (charging)

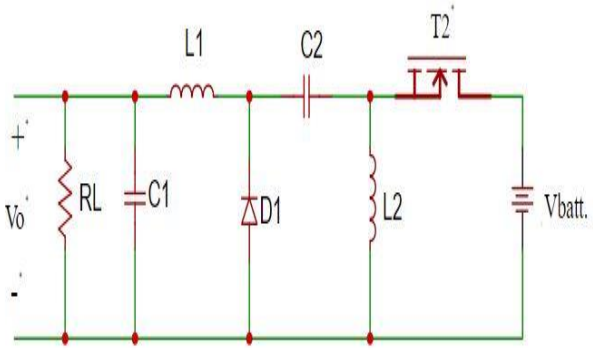

Figure 2b ZETA mode (discharging)

It is essentially a reorganization of the Cuk converter. The output voltage of a SEPIC/ZETA converter can be greater or lower in both directions, but the polarity of the DC buses remains the same [1]. T1 is the main switch and T2 is the synchronous rectifier in SEPIC mode. T1 is the synchronous rectifier in ZETA mode, and T2 is the main switch [4,13]. To reduce output voltage ripple and voltage stress on switches, inductors L1 and L2 can be coupled. The suggested bidirectional SEPIC-ZETA converter's voltage conversion ratio Vo /Vi can be written as [14]:

$$\frac{V_O}{V_{in}} = \frac{D}{1-D} \tag{1}$$

where ($D = T_{on}/T$) is the duty cycle D of switch T1, and Ton and T are the on-state time and switching period of switch Tl, respectively. The current ripple through L1 has a peak-to-peak value of ΔL_1 that is listed.

$$\Delta L_1 = \frac{V_{in}}{L_1} * T_{on} \tag{2}$$

Furthermore, after the steady-state power balance is achieved so:

$$V_{in} I_{L1} = V_O I_O \tag{3}$$

Equations (2) and (3) will yield:

$$\frac{I_{L1}}{I_O} = \frac{D}{1-D} \tag{4}$$

When T2 is turned on, the inductor current I_{L1} and the inductor current I_{L2} flow simultaneously into T2 to the output side, yielding the equation below [15].

$$I_O = (I_{L1} + I_{L2})(1 - D) \tag{5}$$

Equations (4) and (5) will result in the following:

$$I_{L2} = \frac{1-D}{D} * I_{L1} \ = I_O \tag{6}$$

4. SIMULATION RESULTS

The input power of a DC-DC converter is not always equal to the output power because part of the power is dissipated as heat [14,16]. The junction temperature and total power absorbed by a transistor may be calculated as:

$$\Delta T = R_{th} * P_{diss.} - T_a \tag{7}$$

$$P_{diss} = V_{ds} * I_{ds} \tag{8}$$

The overall switching loss for the converter was expressed as

$$P_{switch} = \frac{(E_{sw(on)} + E_{sw(off)}) * f_s}{2} \quad (9)$$

Where fs is switching frequency, $E_{sw(on)}$ is the energy losses during duration of switch-on and $E_{sw(off)}$ is the energy losses of in duration of switch-off. The efficiency of bidirectional efficiency could be obtained as:

$$\eta = \frac{P_o}{P_{in}} = 1 - \frac{P_{LOSS}}{P_{in}} \quad (10)$$

The simulation will be implemented using the PLECS program stand-alone type [17,18], to study the effect of the environmental temperature (25 °C, 40 °C) on the MOSFET junction temperature that is used in the bidirectional SEPIC-ZETA converter. There are two modes of operation for the converter: forward and backward. There are two types of power switches (UJ3C065080K3S and SCT50N120).

4.1 Bidirectional SEPIC-ZETA converter using (UJ3C065080K3S) model

4.1.1 Forward mode (SEPIC mode)

The simulation parameters for this mode are listed in Table 1.

Table 1 simulation parameters [3]

Parameter	T=25°C	T=40°C
Vin	48V	48V
C2	40µF	40µF
C3	470 µF	470 µF
L1,L2	133µH	133µH
R_L	6Ω	6Ω
Duty ratio	0.63	0.63
Freq.	40KHz	40KHz

Figure (3) depicts the output waveforms for output voltage and input current.

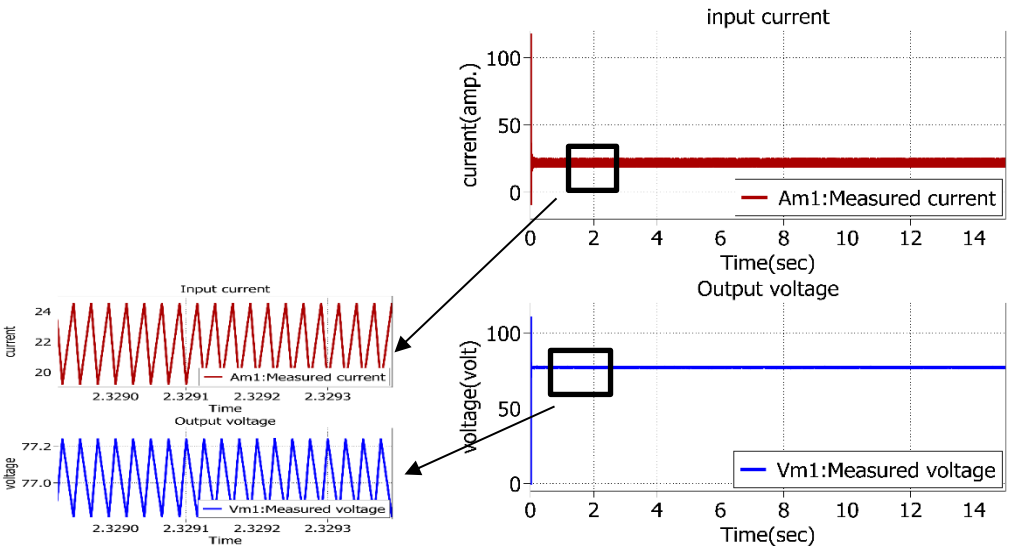

Figure 3 Input current and Output voltage (forward mode)

The model datasheet was used to determine the internal component values for power switches [19,20]. The MOSFET and diode's conduction and switching losses, as well as heat flow meters from a thermal model, are all taken into account. The conduction and switching losses of the MOSFET and diode, as well as the heat flow meter readings and the total of these losses, could be seen in Figure.4**.**

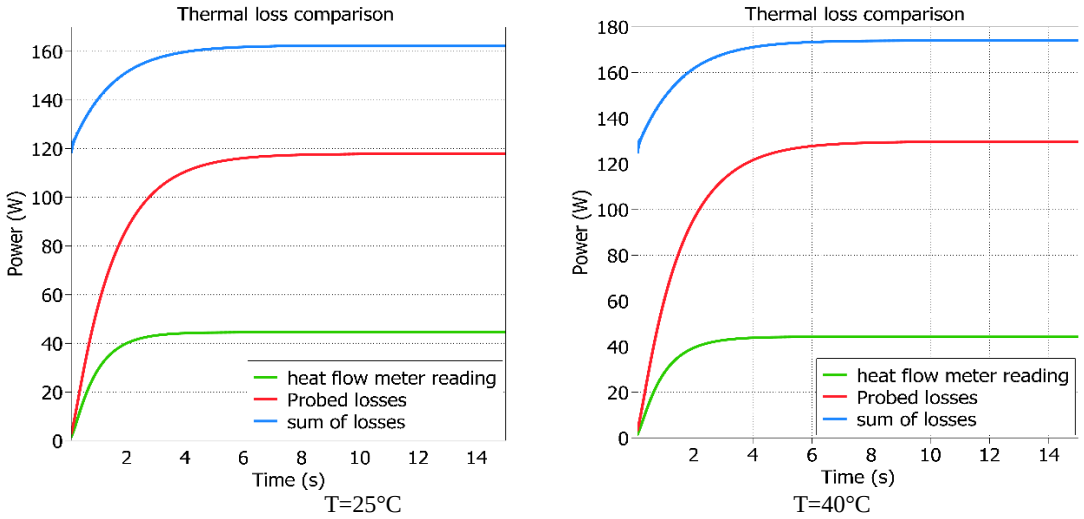

T=25°C T=40°C

Figure 4 Thermal losses

As can be seen in Table (2), efficiency declined by 1.1 % as the ambient temperature is raised and losses increased.

Table 2 Simulation results

Simulation Results	T=25°C	T=40°C
V_{out} (volt)	77.24V	77.24V
Input current(amp.)	24.5A	24.5A
Efficiency (%)	84.54	83.44
Probed losses (w)	117.85	129.6
Heat flow meter reading (w)	44.5	44.3
Sum losses(w)	162.36	174

The MOSFET junction temperature and diode junction temperature are displayed in Figures (5), (6) for both ambient temperature (T = 25 °C, T = 40 °C).

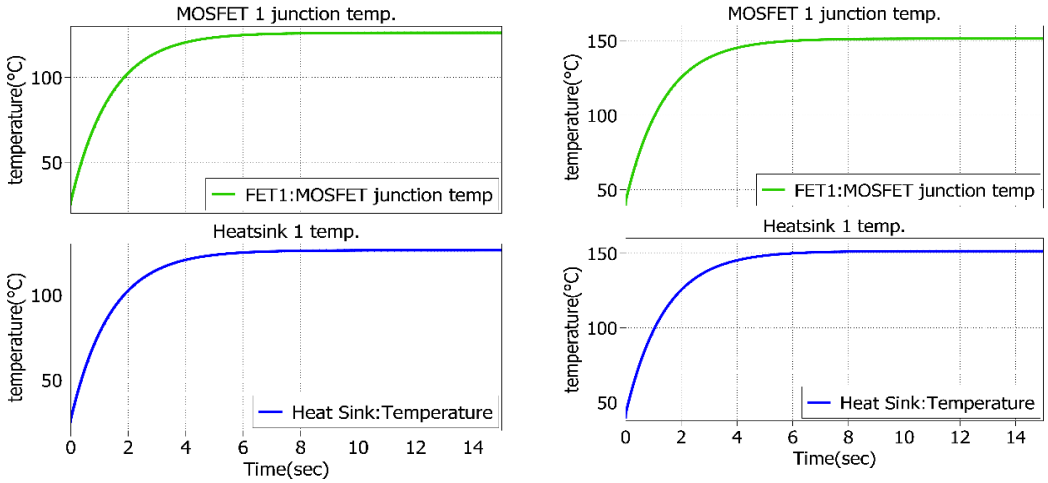

(a)T=25°C (b) T=40°C

Figure 5. MOSFET junction and heatsink temperature

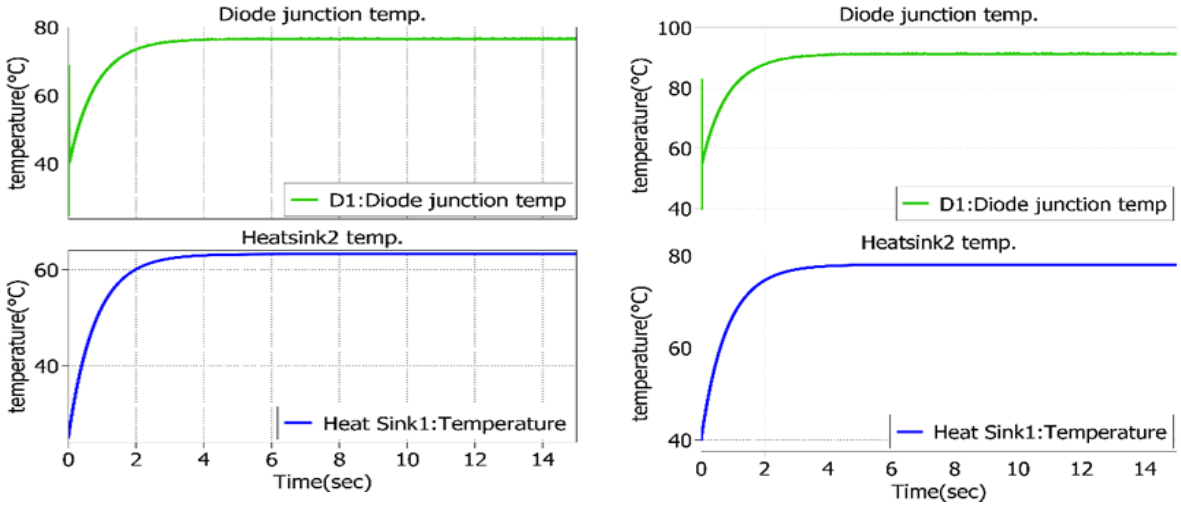

(a) T=25°C (b) T=40°C

Figure 6 Diode junction and heatsink temperature

The temperature readings of the MOSFET, the diode junction, and the heatsink are listed in Tables (3), (4).

Table 3 Reading of the junction temp. and heatsink temp.

	T=25°C	T=40°C
MOSFET junction temp.(°C)	**126.2**	**151.38**
Heatsink1 temp.(°C)	**126.2**	**151.38**

Table 4 Diode junction and heatsink temperature

	T=25°C	T=40°C
Diode junction temp.(°C)	**76.54**	**91.34**
Heatsink2 temp.(°C)	**63.2**	**78**

4.1.2 Backward mode (ZETA mode)

In this mode, the simulation parameters are stated in Table (5).

Table 5 Simulation parameters [3]

Parameter	T=25°C	T=40°C
Vin	**48V**	**48V**
C2	**40µF**	**40µF**
L1,L2	**133µH**	**133µH**
R_L	**6Ω**	**6Ω**
Duty ratio	**0.63**	**0.63**
Freq.	**40KHz**	**40KHz**

At time of (15) second, the output waveforms for output voltage and input current are shown in Figure (7).

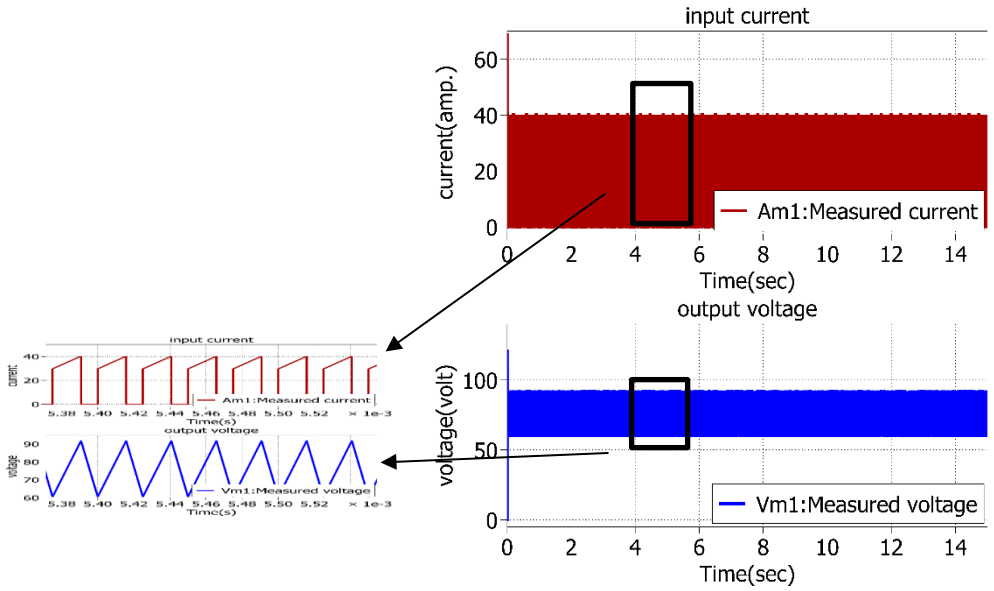

Figure 7. Output voltage and input current waveforms(backward mode)

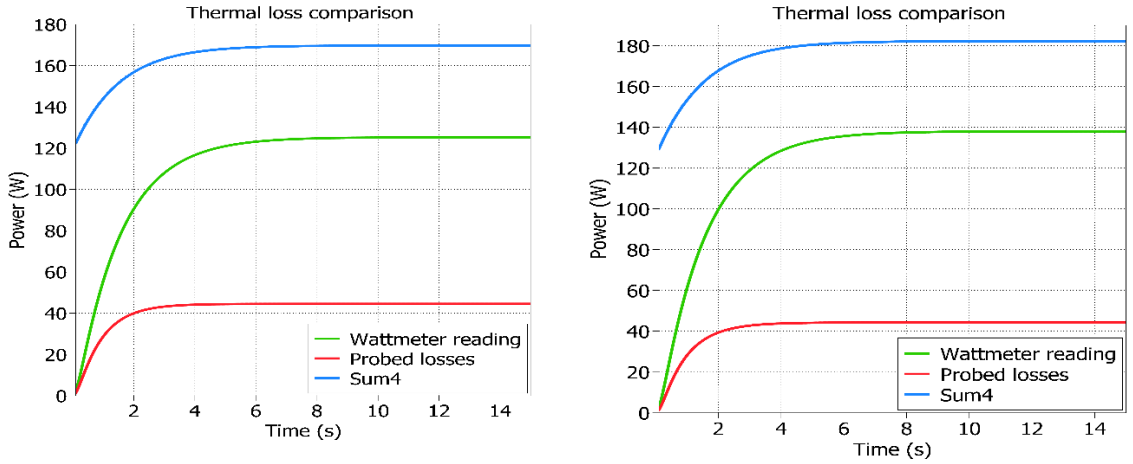

T=25°C T=40° C

Figure 8 Thermal losses

Figure 8 shows the MOSFET and diode conduction and switching losses, as well as the heat flow meter values and the sum of these losses.

Table 6 Simulation results

Simulation results	T=25°C	T=40°C
V_{out} (volt)	91.6V	91.6V
Input current (amp.)	40.1A	40.1A
Efficiency (%)	84.06	82.88
Probed losses(w)	44.5	44.2
wattmeter reading(w)	125.2	137.9
Sum losses(w)	169.7	182.2

As can be seen in Table (6), efficiency decreased by 1.18% and losses increased as the ambient temperature increased.

Figures (9), (10) shows the MOSFET junction temperature and diode junction temperature for each ambient temperature (T = 25 °C, T = 40 °C).

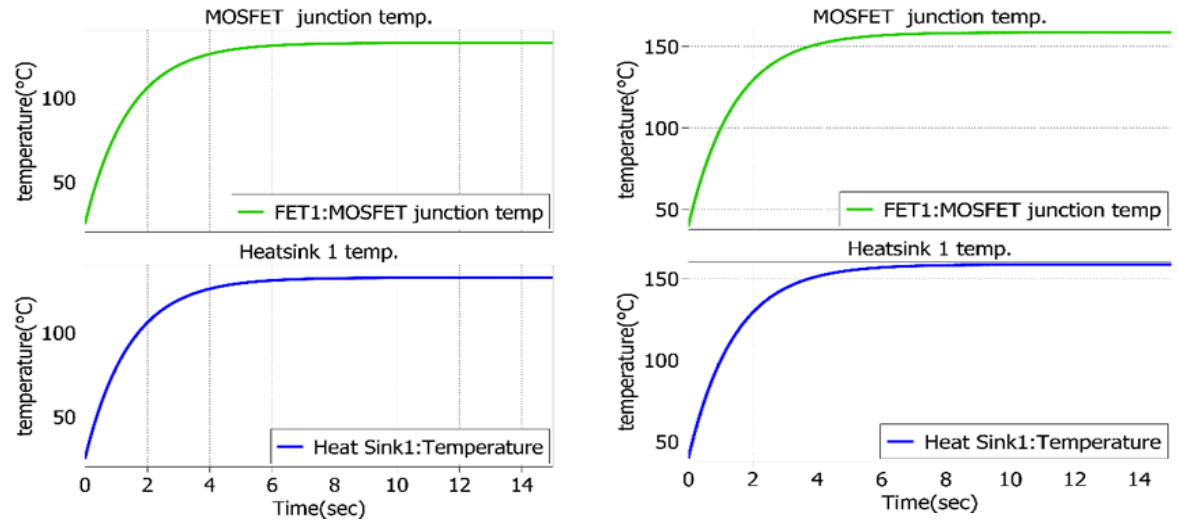

(a)T=25°C (b) T=40°C

Figure 9 MOSFET junction and heatsink temperature

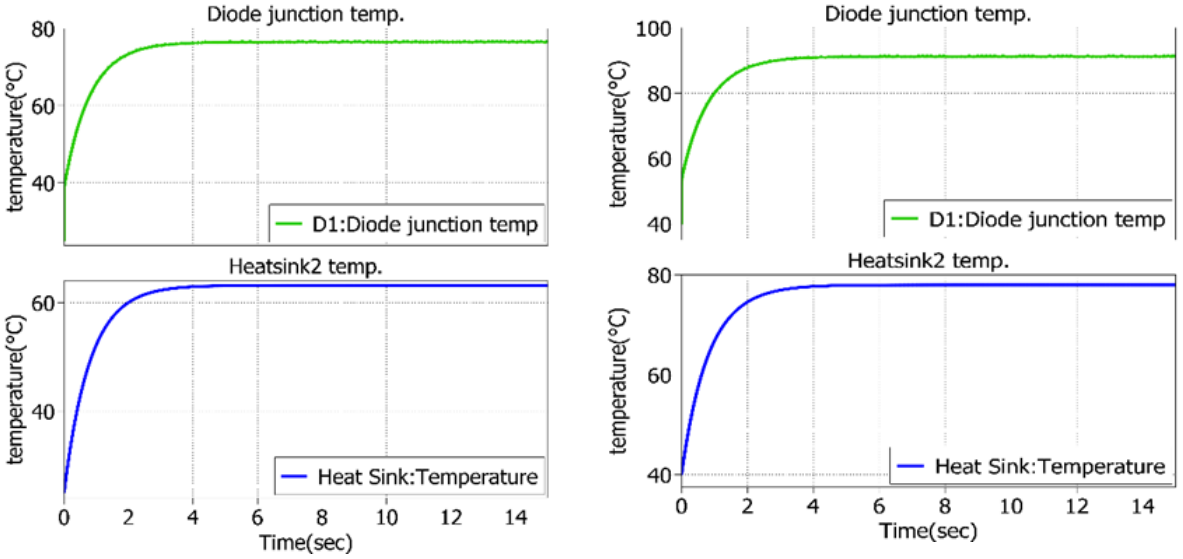

(a) T=25°C (b) T=40°C

Figure 10 Diode junction and heatsink temperature

The temperatures readings of the MOSFET and diode junction and the heatsink are listed in the Tables (7), (8).

Table 7 MOSFET junction and heatsink temperature readings

	T=25°C	T=40°C
MOSFET junction temp.(°C)	**132.5**	**158.5**
Heatsink1 temp. (°C)	**132.5**	**158.5**

Table 8 Diode junction and heatsink temperature readings

	T=25°C	T=40°C
Diode junction temp. (°C)	**76.5**	**91.2**
Heatsink2 temp. (°C)	**63.2**	**77.9**

4.2 Bidirectional SEPIC-ZETA converter using (SCT50N120) model

4.2.1 Forward mode (SEPIC mode)

The simulation parameters for this mode are listed in Table 9.

Table 9 Simulation parameters [3]

Parameter	T=25°C	T=40°C
Vin	**48V**	**48V**
C2	**40µF**	**40µF**
C3	**470 µF**	**470 µF**
L1,L2	**133µH**	**133µH**
R_L	**6Ω**	**6Ω**
Duty ratio	**0.63**	**0.63**
Freq.	**40KHz**	**40KHz**

Figure (11) depicts the output waveforms for output voltage and input current.

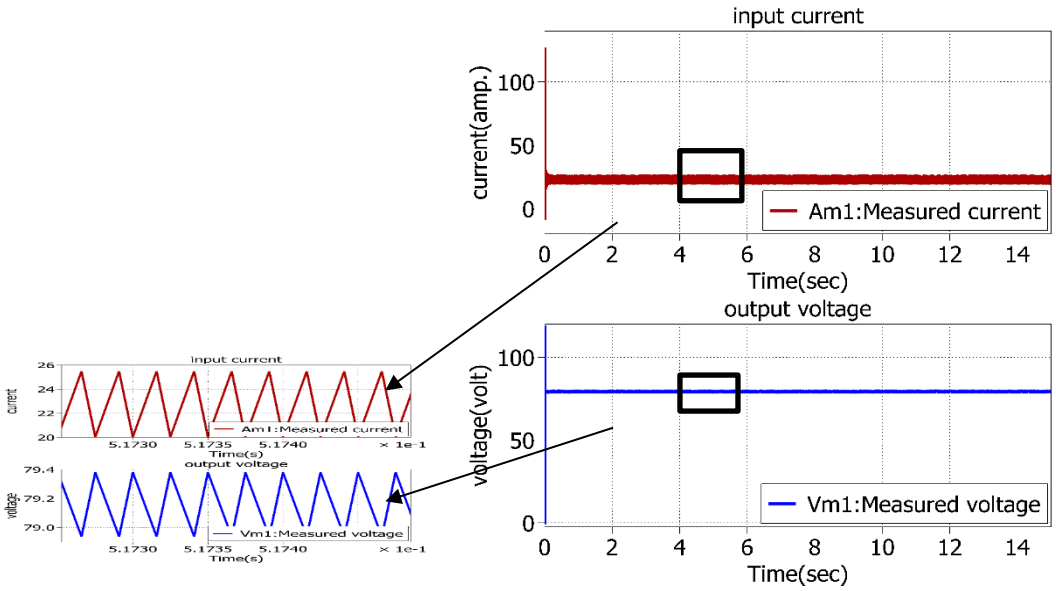

Figure 11. Input current and output voltage (forward mode)

The conduction and switching losses of the MOSFET and diode, as well as the heat flow meter readings and the total of these losses, could be seen in Figure (12).

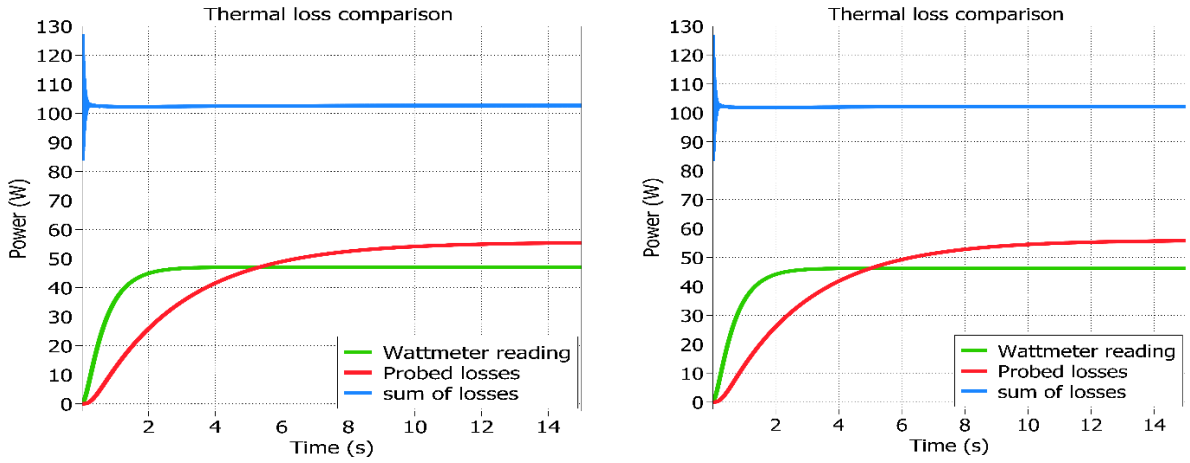

Figure 12. Thermal losses

As can be seen in Table (10), efficiency decreased by 0.05 % as the ambient temperature is raised and losses decreased.

Table 10 Simulation results

Simulation Results	T=25°C	T=40°C
V_{out} (volt)	79.3V	79.3V
Input current (amp.)	25.5A	25.5A
Efficiency (%)	90.61	90.56
Probed losses (w)	55.4	55.7
Wattmeter reading (w)	47	46.23
Sum losses (w)	102.66	102.3

The MOSFET junction temperature and diode junction temperature are displayed in Figures (13), (14) for each ambient temperature (T = 25 °C, T = 40 °C).

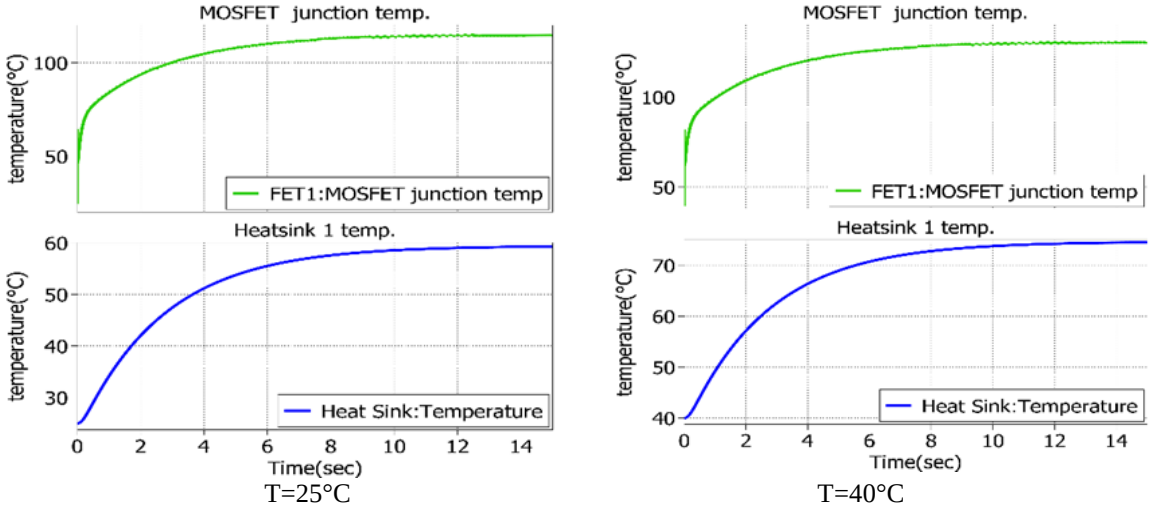

Figure 13 MOSFET junction and heatsink temperature

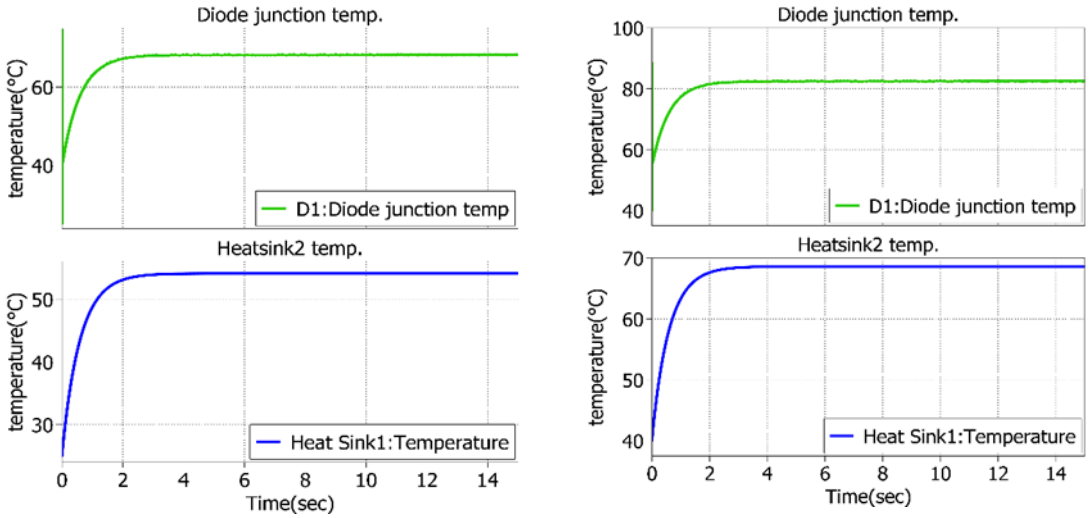

(a) T=25°C (b) T=40°C

Figure 14 Diode junction and heatsink temperature

temperatures readings of the MOSFET and diode junction and the heatsink are listed in the Tables (11), (12).

Table 11 Reading of the junction temp. and heatsink temp.

	T=25°C	T=40°C
MOSFET junction temp. (°C)	**115**	**130.6**
Heatsink1 temp. (°C)	**59.2**	**74.5**

Table 12 Diode junction and heatsink temperature

	T=25°C	T=40°C
Diode junction temp. (°C)	**68.2**	**82.44**
Heatsink2 temp. (°C)	**54.1**	**68.66**

4.2.2 Backward mode (ZETA mode)

The simulation parameters are listed in Table (13) in this mode.

Table 13 Simulation parameters [3]

Parameter	T=25°C	T=40°C
Vin	**48V**	**48V**
C2	**40µF**	**40µF**
L1,L2	**133µH**	**133µH**
R	**6Ω**	**6Ω**
Duty ratio	**0.63**	**0.63**
Freq.	**40000HZ**	**40000HZ**

Figure (15) shows the output waveforms for output voltage and input current.

.

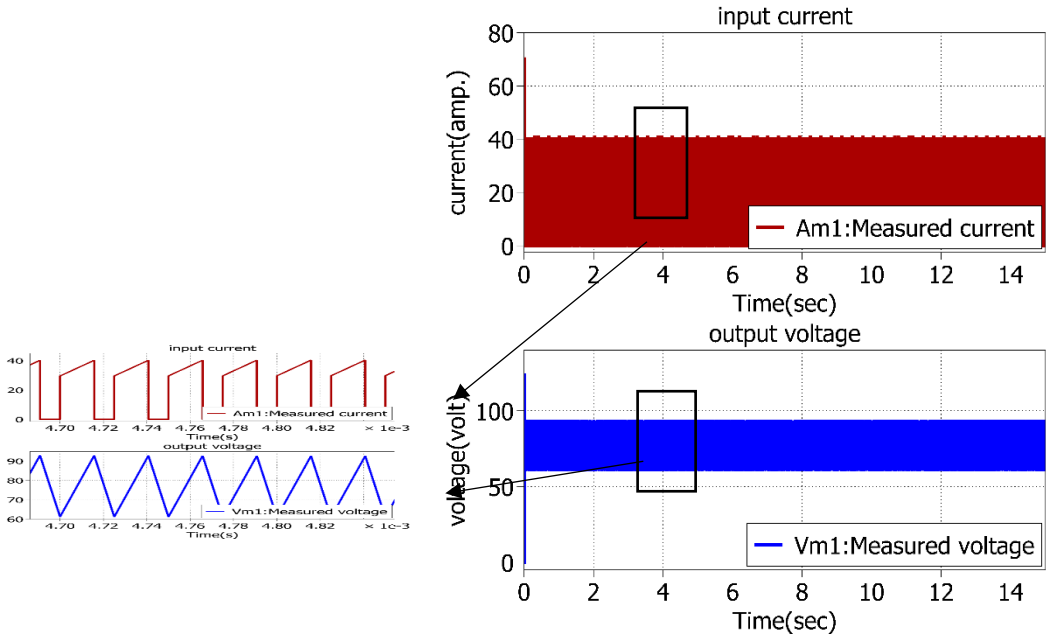

Figure 15 .Output voltage and input current waveforms (backward mode)

Figure (16), shows the heat flow meter readings, the conduction and switching losses of the MOSFET and diode, as well as the sum of these losses.

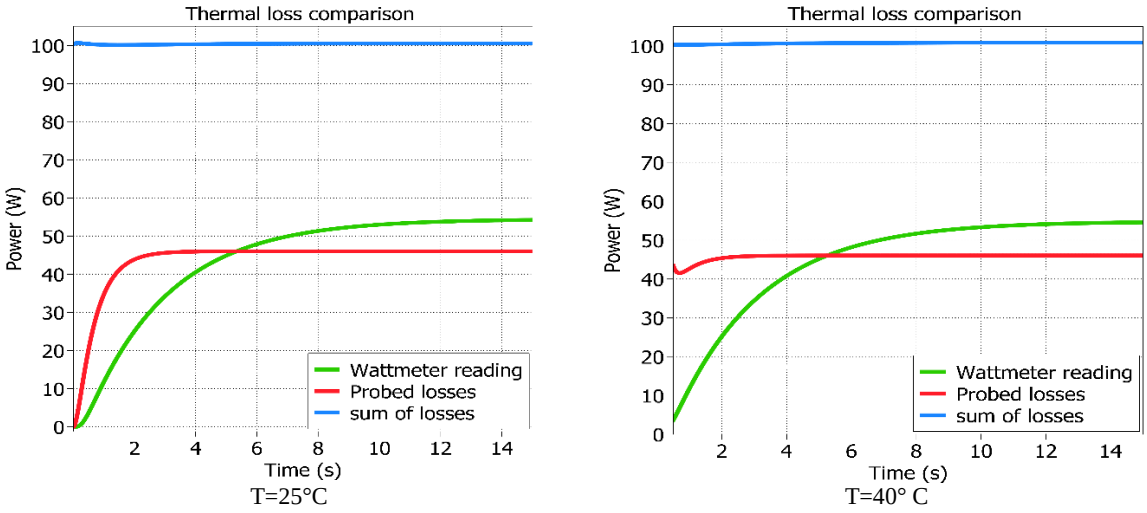

Figure 16 Thermal losses

As seen in Table (14), as the ambient temperature increased, efficiency increased by 0.04% and losses slightly decreased.

Table 14 Simulation results

Parameter	T=25°C	T=40°C
V_{out} (volt)	93V	93V
Input current (amp.)	40.7A	40.7A
Efficiency (%)	90.7	90.74
Probed losses (w)	46	45.25
Wattmeter reading (w)	54.2	54.58
Sum losses (w)	100.5	100.1

Figures (17), (18) shows the MOSFET junction temperature and diode junction temperature for each ambient temperature (T = 25 °C, T = 40 °C).

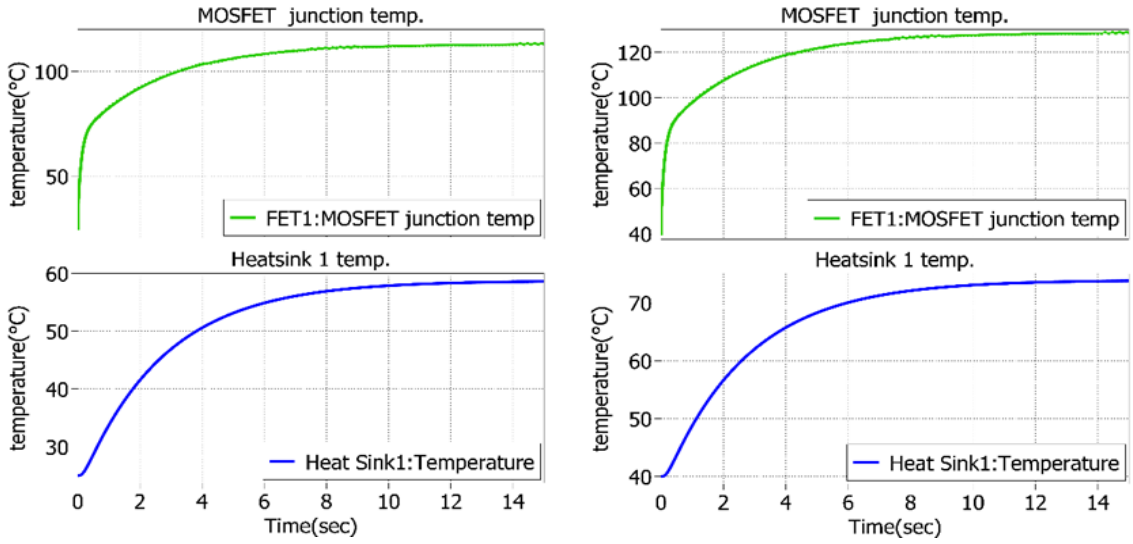

T=25°C T=40°C

Figure 17 MOSFET junction and heatsink temperature

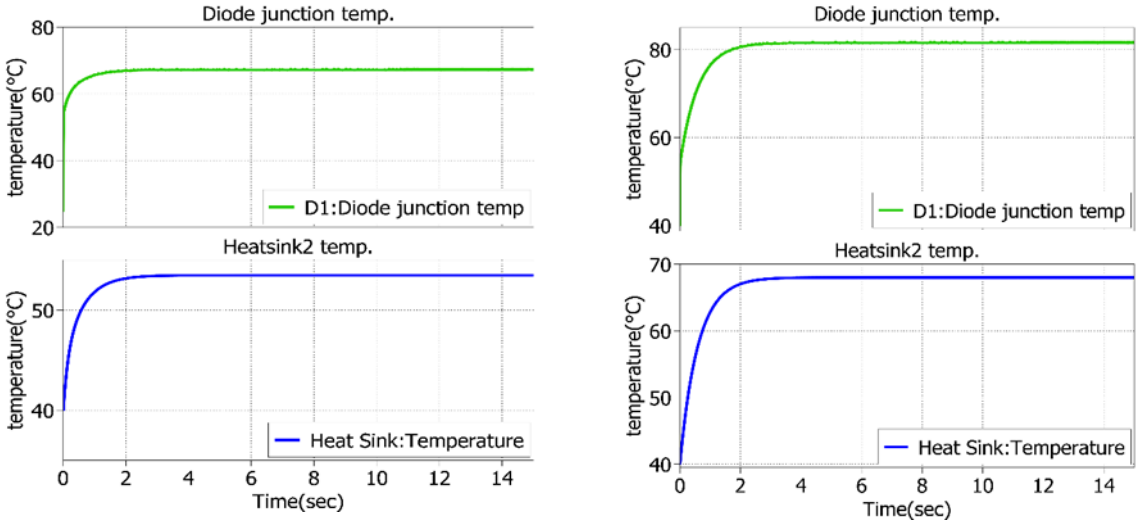

T=25°C T=40°C

Figure 18 Diode junction and heatsink temperature

Temperatures readings of the MOSFET and diode junction and the heatsink are listed in the Tables (15), (16).

Table 15 MOSFET junction and heatsink temperature readings

	T=25°C	T=40°C
MOSFET junction temp. (°C)	113.23	128.7
Heatsink1 temp.(°C)	58.58	73.78

Table 16 Diode junction and heatsink temperature readings

	T=25°C	T=40°C
Diode junction temp.(°C)	67.33	81.6
Heatsink2 temp.(°C)	53.5	68

Figure (19) shows a comparison of the MOSFET models, the first model (UJ3C065080K3S) and the second model (SCT50N120), that will be utilized in the SEPIC-ZETA converter for two modes of operation (SEPIC mode and ZETA mode), based on the MOSFET junction temperature for two ambient temperatures (25 °C and 40 °C).

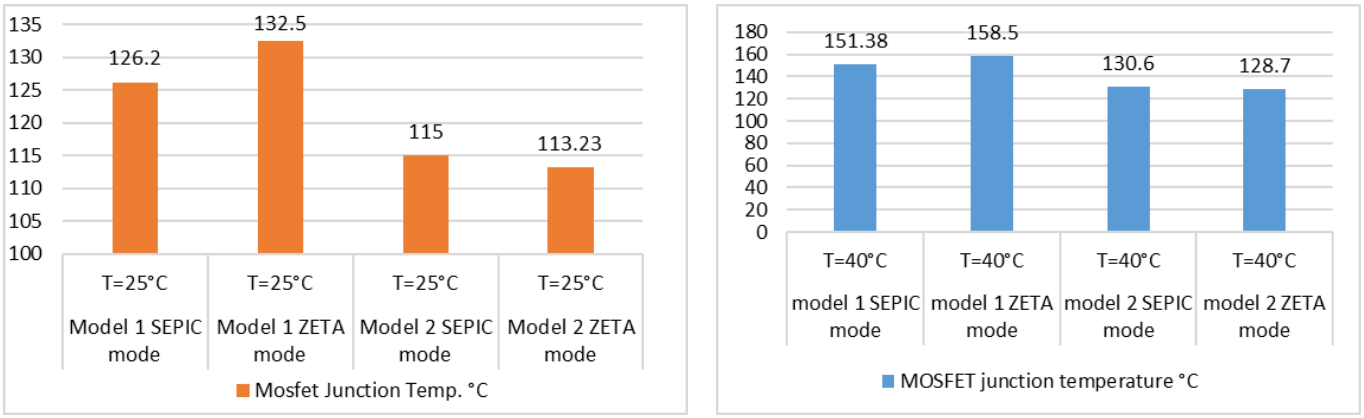

Figure 19 Comparison of MOSFET junction temperature for two MOSFET models

Figures (20) present a comparison between the two models of MOSFETs, the first model (UJ3C065080K3S) and the second model (SCT50N120), that were used for the bidirectional SEPIC-ZETA converter for two modes of operation (SEPIC mode and ZETA mode), based on the efficiency, probed losses, wattmeter reading, and the sum of losses.

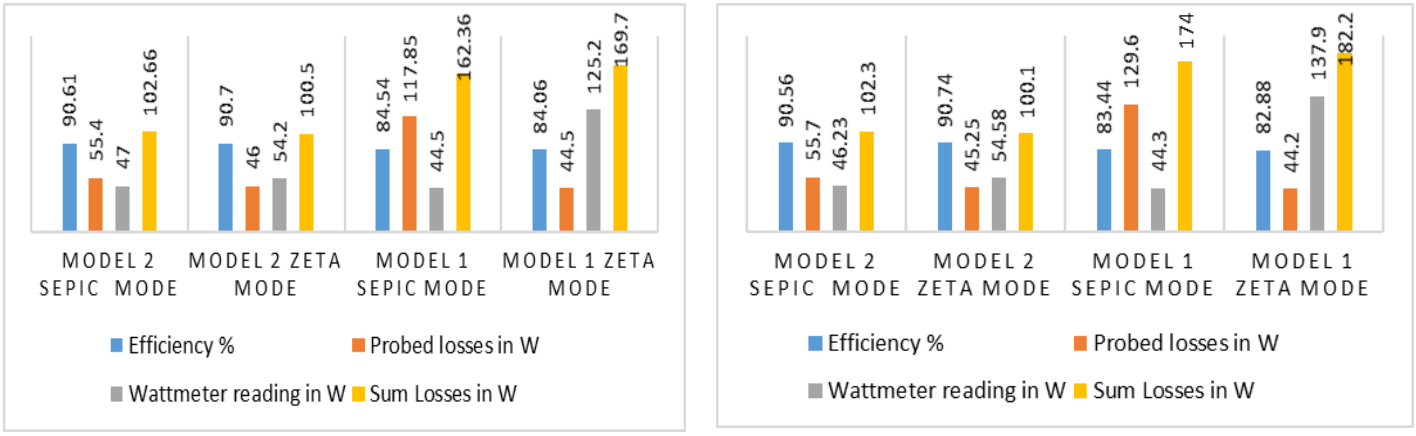

(a) at T=25°C (b) T=40°C

Figure 20 Comparison of two models used in bidirectional DC-DC converter (efficiency and losses)

Both figures are used to select a better MOSFET model for better performance of the bidirectional SEPIC-ZETA converter based on the selected conditions.

5. CONCLUSIONS

This paper provides acomparison for the performance of the circuit based on two MOSFET models, depending on the MOSFET junction temperature and power switch model utilized for selecting the suitable MOSFET for the SEPIC-ZETA converter suitable for Iraqi summer temperatures that could reach 40°C and offering the best performance. According to simulation results, the junction temperature of the MOSFET was 151.38 in the forwarding mode and for the first model (UJ3C065080K3S) at T = 40 °C, while the MOSFET junction temperature was 158.5 °C in the reverse mode. In the second model (SCT50N120) and for the same T = 40°C, the MOSFET junction temperature exceeds 130.6°C in the forwarding mode. The converter's junction temperature was 128.7 °C when in backward mode. As can be seen, the bidirectional SEPIC-ZETA converter performs better in the second model of the MOSFET (SCT50N120).

REFERENCES

1. Tytelmaier, K., Husev, O., Veligorskyi, O., & Yershov, R. (2016). “A review of non-isolated bidirectional DC-DC converters for energy storage systems”. *2016 II International Young Scientists Forum on Applied Physics and Engineering (YSF)*.
2. Hadi Tarzamni, Farzad Tahami, Mahmud Fotuhi-Firuzabad, Frede Blaabjerg, “Improved Markov Model for Reliability Assessment of Isolated Multiple-Switch PWM DC-DC Converters”, *IEEE Access*, 10.1109/ACCESS.2021.3060950, 9, (33666-33674), (2021).
3. Kim, I.-D., Young-Ho Lee, Byoung-Ho Min, Nho, E.-C., & Ahn, J.-W. (2007). “Design of bidirectional PWM SEPIC/Zeta DC-DC converter”. *2007 7th international Conference on Power Electronics*. https://doi.org/10.1109/icpe.2007.4692461.
4. Song, M.-S., Son, Y.-D., & Lee, K.-H. (2014). “Non-isolated bidirectional soft-switching SEPIC/ZETA converter with reduced ripple currents”. *Journal of Power Electronics*, *14*(4), 649–660. https://doi.org/10.6113/jpe.2014.14.4.649.
5. Hamirpur, N. I. T., & Pradesh, H. “bi-directional converter topology for solar battery charging”. *International Research Journal of Modernization in Engineering Technology and Science*, *02*(09), 12–17(2020).
6. M. Shahjalal, M. R. Ahmed, H. Lu, C. Bailey, and A. J. Forsyth, "An Analysis of the Thermal Interaction Between Components in Power Converter Applications," in *IEEE Transactions on Power Electronics*, *35*(9), pp. 9082-9094, Sept. 2020, DOI: 10.1109/TPEL.2020.2969350.
7. Sunarno, E., Sudiharto, I., Nugraha, S. D., Murdianto, F. D., Suryono, & Qudsi, O. A. (2019). “Design and implementation bidirectional SEPIC/ZETA converter using Fuzzy Logic Controller in DC Microgrid Application”. *Journal of Physics: Conference Series*, *1367*(1), 012058. https://doi.org/10.1088/1742-6596/1367/1/012058.

8. S. Gurudiwan, S. K. Roy and K. Basu, "Design and Implementation of 1.5 kW Half Bridge Bidirectional DC-DC Converter based on Gallium Nitride devices," *2019 National Power Electronics Conference (NPEC)*, 2019, pp. 1-6, doi: 10.1109/NPEC47332.2019.9034802.
9. Dusmez, Serkan, Amin Hasanzadeh, and Alireza Khaligh. "Loss analysis of non-isolated bidirectional DC/DC converters for hybrid energy storage system in EVs." *2014 IEEE 23rd International Symposium on Industrial Electronics (ISIE)*. IEEE, 2014.
10. Wang, Chun et al. “Efficiency analysis of a bidirectional DC/DC converter in a hybrid energy storage system for plug-in hybrid electric vehicles.” *Applied Energy 183* (2016): 612-622.
11. Dini P, Saponara S. “Electro-Thermal Model-Based Design of Bidirectional On-Board Chargers in Hybrid and Full Electric Vehicles”. *Electronics*. 2022; *11*(1):112. https://doi.org/10.3390/electronics11010112.
12. Diana Denny C, & Shahin M. (2015). “Analysis of bidirectional SEPIC/ZETA converter with coupled inductor”. *2015 International Conference on Technological Advancements in Power and Energy (TAP Energy)*. https://doi.org/10.1109/tapenergy.2015.7229600.
13. M. Shunmathi, J. Gnanavadivel and S. T. Jaya Christa, "Power Factor Correction with Single Stage AC-DC Non-Isolated Zeta Converter Fed SRM Drive," *2021 7th International Conference on Electrical Energy Systems (ICEES)*, 2021, pp. 95-100, DOI: 10.1109/ICEES51510.2021.9383693.
14. Gayen, P. K., Roy Chowdhury, P., & Dhara, P. K. (2018). An improved dynamic performance of bidirectional SEPIC-Zeta converter based battery energy storage system using adaptive sliding mode control technique. *Electric Power Systems Research*, *160*, 348–361. https://doi.org/10.1016/j.epsr.2018.03.016.
15. Reddy, B. M., & Samuel, P. (2016). A comparative analysis of non-isolated bi-directional dc-dc converters. 2016 *IEEE 1st International Conference on Power Electronics, Intelligent Control and Energy Systems (ICPEICES)*. doi:10.1109/icpeices.2016.7853292.
16. Malev, Evgeni. "Thermal model of bidirectional DC/DC converter.". *ELECTROTECHNICA & ELECTRONICA, E+E*, 56. pp 20-28.
17. Plecs. Plexim. (2022, August 31). Retrieved July 27, 2022, from https://www.plexim.com/products/plecs.

18. Plexim Plecs Manual - [PDF document]. vdocuments.net. (N.D.). Retrieved July 27, 2022, from https://vdocuments.net/plexim-plecs-manual.html
19. DATASHEET description uj3c065080k3s - united sic. (N.D.). Retrieved July 27, 2022, from https://unitedsic.com/datasheets/DS_UJ3C065080K3S.pdf.
20. Alldatasheet.com. (N.D.). SCT50N120 PDF, SCT50N120 description, SCT50N120 Datasheet, SCT50N120 view: All datasheet: all datasheet. Retrieved July 27, 2022, from https://pdf1.alldatasheet.com/datasheet-pdf/view/930637/STMICROELECTRONICS/SCT50N120.html.